Hindawi Publishing Corporation
Journal of Nanomaterials
Volume 2015, Article ID 291248, 9 pages
http://dx.doi.org/10.1155/2015/291248

Research Article

Mechanical, Thermal, and Microstructural Analysis of Polyvinyl Alcohol/Montmorillonite Nanocomposites

P. G. Allison,[1] R. D. Moser,[2] M. Q. Chandler,[2] J. A. Caminero-Rodriguez,[3] K. Torres-Cancel,[2] O. G. Rivera,[1] J. R. Goodwin,[4] E. R. Gore,[2] and C. A. Weiss Jr.[2]

[1]*Department of Mechanical Engineering, University of Alabama, Tuscaloosa, AL 35487, USA*
[2]*Geotechnical and Structures Laboratory, US Army Engineer Research & Development Center, Vicksburg, MS 39180, USA*
[3]*Department of Chemical Engineering, University of Puerto Rico at Mayagüez, PR 00680, USA*
[4]*Central Analytical Facility, University of Alabama, Tuscaloosa, AL 35487, USA*

Correspondence should be addressed to P. G. Allison; pallison@eng.ua.edu

Received 2 January 2015; Accepted 18 March 2015

Academic Editor: Sheng-Rui Jian

Structural biomaterials such as nacre, bone, and fish scales possess unique structures that have hierarchical spatial configurations, which provide excellent mechanical properties when compared to their individual constituents. These observations have been the motivation for designing and characterizing bioinspired materials with high strength, high stiffness, and corrosion-resistant properties while at the same time being environmentally friendly. It has been demonstrated that polymer-clay nanocomposites can simulate the behavior of nacreous biomaterials such as abalone shell. Mechanical, thermal, and microstructural analyses characterized solution-cast polyvinyl alcohol (PVA)/montmorillonite (MMT) nanocomposite properties over compositions ranging from the neat polymer to 25% volume fraction of MMT nanoclay. Uniaxial tensile experiments were performed at displacement rates of 1 mm/min and 50 mm/min. Strength values are similar to those shown by nacre and represent a homogeneous dispersion of the MMT in the polymer matrix. Strength-to-weight ratios are similar to many structural metals.

1. Introduction

Natural biocomposite materials such as nacre [1–3], bone [4, 5], horn [5, 6], and mineralized fish scales [7–10] are comprised of inorganic/organic nanocomposites with excellent mechanical properties, which have been inspirations for the development of man-made nanocomposites. Specifically, the nacre design is a nanocomposite with a brick and mortar morphology composed of aragonite nanoscale constituent tablets measuring approximately eight microns in length and width, 500 nm in thickness [1–3]. The nanoscale constituent tablets are bonded by tens of nanometers thick organic material composed of proteins and polysaccharides [1–3]. The arrangement of the aragonite in the structure has been reported as being layered with a 33% overlap region of the tablet surfaces and then a core region of the tablet, in which each region experiences different stress state [3]. According to Gao [11], the nanoscale tablet constituents do not fracture during loading because of the nanoscale flaw tolerance, which is likely why nature chooses to use nanoscale constituents as the basic building blocks in these types of hierarchical material designs. Different types of polymers and nanoscale reinforcing particles have been used to synthesize the various bioinspired nanocomposites [12–22] reported in the literature to date. Polyvinyl alcohol (PVA) is a biodegradable polymer with excellent physical properties and chemical resistance with wide applications in the adhesive, paper, and textile industries. Montmorillonite (MMT) is a 2 : 1 layered aluminosilicate (or phyllosilicate) clay of the smectite group, consisting of two external silica tetrahedron and a central octahedral sheet of alumina with a layer thickness of approximately 1 nm. This layered structure has large surface area, high stiffness, and high strength [23, 24]. MMT is hydrophilic in its natural state, and PVA is highly soluble in water at elevated temperature. Hydrogen bonds between hydroxyl groups of the PVA and the negatively charged clay

surface [25] can be formed if MMT is properly dispersed in the PVA solutions. PVA/MMT nanocomposites have been synthesized by using Layer-by-Layer (LBL) assembly [16], simple vacuum filtration [26], doctor-blading [27], solution casting [28], and water-evaporation-induced assembly method [20]. The synthesized nanocomposites not only show large improvement on mechanical properties compared to pure PVA but also exhibit excellent properties in flame resistance, barrier, and optical clarity [26]. These methods have advantages and disadvantages as described in Wang et al. [20]. For example, both LBL and evaporation methods have good control on the dispersion of clay particles, but they are time-consuming. Doctor-blading method is time-consuming and also has less control on dispersion.

In this work, a simple solution casting method was developed to improve the dispersion of clay in the PVA polymer matrix. Nanocomposites with different concentrations of MMT were synthesized. Thermogravimetric analysis (TGA) was performed to investigate the effects of MMT concentration, micro-, and nanostructures on the thermal degradation of the nanocomposites. Transmission Electron Microscopy (TEM) and X-ray diffraction (XRD) were performed to investigate the clay dispersion, micro-, and nanostructure of the nanocomposites. Uniaxial tension tests were performed to probe the bulk mechanical properties of the nanocomposites at different concentrations of MMT and at different rates of loading. Most past studies [13, 14, 19, 20, 29, 30] focused on correlating the modulus and strength improvement of nanocomposites to the morphologies of the nanocomposites (e.g., nanoclay exfoliation and intercalation). In this work, the effects of clay dispersion, micro-, and nanostructure on the stress-strain curves of the nanocomposites under different rate of loading were discussed to gain understanding on the complex interactions between nanoscale platelets and polymer chains.

2. Experimental Methods

2.1. Materials and Reagents. Polyvinyl alcohol (PVA/$(C_2H_4O)_x$) 99.7% hydrolyzed with an average molecular weight of 115,000 g/mol was obtained from Scientific Polymer Products. Nanoclay, hydrophilic bentonite (MMT/$(Na, Ca)_{0.3}(Al, Mg)_2Si_4O_{10}(OH)_2 \cdot n(H_2O)$), with a molecular weight of 180.1 g/mol and an average particle size of $\leq 25\,\mu$m, was purchased from Sigma-Aldrich. All the chemicals used in this study were of analytical grade and used without further purification.

2.2. Preparation of PVA/MMT Composites

2.2.1. Presynthesis Treatment of PVA/MMT. First, 20 grams of hydrolyzed PVA and MMT was weighed and placed in a lab furnace at 36°C for 24 hr to remove the excess moisture content, before starting the composite synthesis.

2.2.2. Synthesis of PVA/MMT through a Solution-Intercalation Method. In this method the nanocomposites films were prepared by the solution-intercalation film-casting method [19]. In a typical process to prepare a 1 vol.% MMT solution, a mass balance was performed (Table 1) to calculate the required amount in grams of required PVA and MMT (5 wt.% dissolved solids). After weighing 0.46 grams of MMT it was dispersed in deionized water and left to stir (IKA RW 20 overhead stirrer) for 24 hr followed by sonication for 30 min. The solution was heated to 90–94°C and 24.54 grams of PVA was dissolved. A volume of 21 mL of solution was cast in a polyethylene dish and was left to dry in an incubator at 40°C and 25% relative humidity (RH) for 72 hr.

Table 1: MMT/PVA amounts in grams utilized for the preparation of 500 grams of solution.

Volume fraction MMT	MMT (grams)	PVA (grams)
1	0.4611	24.5389
3	1.3602	23.6398
5	2.2297	22.7703
10	4.2827	20.7173
25	9.5694	15.4306

2.2.3. Synthesis of PVA/MMT through Modified Solution-Intercalation Method. The modification of the previous method involved the configuration of the solution processing stages and variables. It contributed to a better exfoliation of the MMT nanoclay in water before adding the PVA. First, the appropriate amount of MMT was weighed and added to the solution followed by stirring for 24 hr. After stirring, the solution was subjected to three cycles of sonication and stirring of 30 min and 2 hr, respectively. The solution was heated to 90–94°C and the PVA was added to the solution. Once the polymer was dissolved, the solution was left to stir at the same temperature for 5 min. Finally, the solution was cooled down at ambient temperature, while mixing. With a digital pipette, 21 mL was cast in a polyethylene dish and was left to dry for 36 hr in a lab furnace at 40°C and 10% RH.

2.3. Thermogravimetric Analysis (TGA). A Jupiter STA 449 F1 TGA from Netzsch examined the nanocomposite thermal properties using a heating rate of 10°C/min and a temperature range from 30 to 550°C to examine the decomposition rate of the material as a function of clay volume fraction. Ceramic crucibles and a nitrogen gas atmosphere were used for all samples during the experiments.

2.4. X-Ray Diffraction (XRD) Measurements. X-ray diffraction patterns were gathered from an X'Pert Pro Multipurpose Powder Diffractometer system that used standard techniques for phase identification (PANalytical, Inc.). The run conditions included Co-Kα radiation and scanning with a step size less than 0.002. Collection of the diffraction patterns was accomplished using the PC-based Windows version of X'Pert Pro Data Collector and analysis of the patterns using the Jade 2010 program (Materials Data, Inc.), with patterns from the American Mineralogist Crystal Structure Database (1), International Centre for Diffraction Data (ICDD (2)), and/or the inorganic crystal structure database (ICDS (3)).

2.5. Transmission Electron Microscopy (TEM) of Nanoclay Exfoliation and Dispersion. An FEI Tecnai G2 F20 TEM with an accelerating voltage of 200 kV examined as-cast thin nanocomposite cross-sections held on copper TEM grids. An ultramicrotome prepared the thin sections using a diamond knife. The bright field detector, high-angle annular dark field detector (HAADF), and scanning transmission electron microscope (STEM) mode of the TEM identified nanoclay dispersion and exfoliation in the PVA matrix at the different volume fractions.

2.6. Uniaxial Tensile Experiments. After casting, an ASTM D-412-C die with the assistance of MA Series 3 manual press from Lucris Manufacturing pressed out the tensile specimens. A Zeiss Stereo Discovery V20 microscope provided optical images of the tensile coupons and determined the samples width and thickness.

An Instron E3000 ElectroPuls high-resolution low-load uniaxial testing frame performed the tensile experiments in order to determine the tensile modulus, elongation to failure, yield strength, and ultimate tensile strength of the nanocomposites. Experiments were conducted in triplicate at two different displacement rates, 1 mm/min and 50 mm/min, to examine the rate effect on the different volume fractions.

2.7. Fractographic Analysis Using Scanning Electron Microscopy (SEM). A variable pressure FEI Nova NanoSEM 630 field emission SEM examined the microstructure of the nanocomposites using a variable contrast detector (VCD) in backscatter (BSE) mode and through lens detector (TLD) operated in secondary electron (SE) mode. The specimens were sputter-coated for 30 seconds with gold to mitigate charging on the samples to obtain high-magnification images of the cross-sectional fracture surfaces. The samples were mounted vertically on 90-degree pin stubs with carbon tape and imaged using an accelerating voltage of 10 kV.

3. Results

3.1. Thermal Characterization. Following casting of the nanocomposite films, TGA experimental data produced TGA and DTG curves as depicted in Figure 1.

The curves in Figure 1 identified the fact that the decomposition rate decreases as the concentration of MMT increases in the nanocomposites. The curves also show the decomposition profiles of the nanocomposites characterized by three distinct peaks for all the volume fractions. The first peak, correlating to water evaporation, occurs between ambient temperature and 183 to 200°C. A second peak at approximately 260°C correlates to the first step degradation of polyvinyl alcohol-clay nanocomposite, while the third peak at around 440°C is attributed to the second step decomposition. This demonstrates the added thermal stability the reinforcements give to the nanocomposite compared to pure polyvinyl alcohol [25, 31]. The thermogravimetric curves show a reduction of weight loss for the nanocomposites in the range from 198 to 350°C as the volume fraction of MMT increases as a proof of its resistance to degradation as well as their increased heat resistance. While this is partially due to dilution of the system with exfoliate and intercalated MMT, the presence of high surface area MMT dispersed throughout the PVA improves its stability, resulting in increased melting temperatures.

3.2. XRD Measurements. X-ray diffraction analyses were performed on the intercalated PVA/MMT composites (Figure 2).

The samples included those containing 1, 3, 5, 10, 25, and 100 vol.% MMT. Specimens for XRD analysis were oriented on a substrate in order to delineate the basal spacing of the clay in the composite. At 100 vol.% MMT, the basal spacing is approximately 1.4 nm indicative of a hydrated, mixed cation smectitic (montmorillonitic) clay. At low concentrations of clay the PVA easily intercalates into the interlayer of the clay and expands the structure as indicated by the 1.8 nm d-spacings for 1 and 3 vol.% MMT. As the amount of clay increases to 25 vol.%, the basal spacing shifts to 1.7 nm and increases in intensity due to greater amount of clay in the sample. The shift to lower basal d-spacings suggests that between 5 vol.% and 10 vol.% a saturation state is reached and full intercalation of the MMT with PVA cannot be achieved. It also indicates that, at this concentration of clay, a fairly well-ordered material composite is produced. The shift in position continues at higher clay loadings towards the d-spacing of the 100 vol.% MMT sample of 1.4 nm. Experiments done by Strawhecker and Manias [19] show similar results for their PVA/clay composites and for acidified MMT complexes as given in Ip et al. [32].

3.3. TEM Characterization. Representative TEM bright field images of the extreme nanoclay volume fraction levels of 1 vol.% and 25 vol.% in the PVA, respectively, are shown in Figures 3 and 4.

At the lower nanoclay fraction (1 vol.%) in Figure 3(a) the lower magnified image depicts fewer large agglomerates than the low magnified image in Figure 4(a) of the 25 vol.% MMT sample. The higher magnified image in Figure 3(b) shows much better dispersed individual clay stacks for the 1 vol.% material than for the 25 vol.% shown in Figure 4(b). Rather, the nanoclay (dark spots in the bright field image) in Figure 4(b) still appears to be largely agglomerated.

3.4. Uniaxial Tensile Behavior. Experimental tensile test results with their associated uncertainty error bars for samples tested at displacement rates of 1 mm/min and 50 mm/min are compared in Figures 5(a) and 5(b), respectively. Data shown in Figure 5 represented three tests where fracture either occurred in the gage section or the sample did not fracture. However, not all samples fractured but were tested to the maximum crosshead displacement of the load frame. The elongations to failure error bars for the unfractured specimens extend to the end of the strain axis.

Analysis of the tensile stress-strain behavior of the nanocomposites (Figure 5) indicates that a rate effect is observed on the material's strength for all the volume fractions. With the average ultimate tensile strength (UTS) increased for the higher rate (50 mm/min) versus the lower rate (1 mm/min),

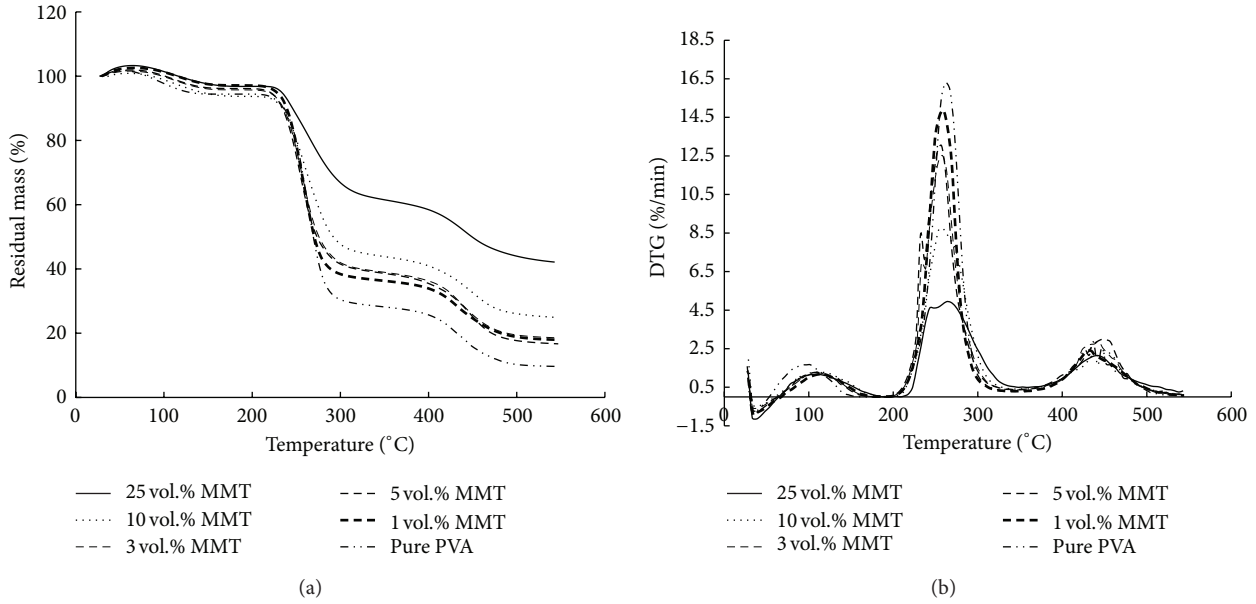

Figure 1: (a) TG and (b) DTG experimental curves for the nanocomposites as a function of MMT concentration.

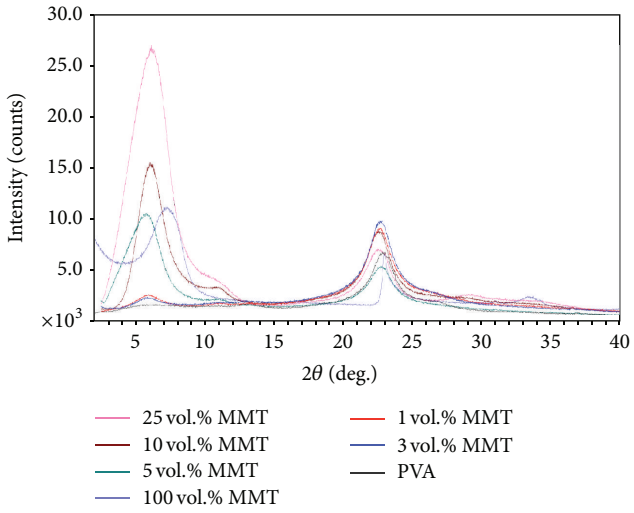

Figure 2: X-ray diffraction patterns for the nanocomposites as a function of MMT concentration.

one would expect strength to typically increase as the rate increases. Examining the phenomenon of the individual volume fractions shows that the 5 vol.% MMT samples exhibited the lowest strength at both testing rates. However, at the lower rate (1 mm/min) the 3 vol.% MMT sample exhibited the highest average UTS, while the 1 vol.% MMT sample produced the highest UTS at the higher rate (50 mm/min). For the 1 mm/min displacement rate, only the 1 and 3 vol.% MMT samples provided a significant improvement over the pure PVA samples. However, for the nanocomposites tested at a displacement rate of 50 mm/min, there was a strength improvement in all the volume fractions except for the 5 vol.% MMT samples. No clear trends on rate effects for the elongation to failure are observable due to the large amount of uncertainty in the data.

Trends in the average, maximum, minimum, and standard deviation tensile modulus for the nanocomposites tested at the two displacement rates are provided in Table 2.

At the low displacement rate of 1 mm/min, the 3 vol.% MMT had the highest average and maximum tensile modulus, while, at a higher displacement rate of 50 mm/min, the 25 vol.% MMT exhibited the highest maximum and average tensile modulus. Interestingly, the average tensile modulus for the 3 and 5 vol.% MMT samples did not show a discernable dependence on testing rate, whereas the pure PVA, 1, 10, and 25 vol.% MMT samples all displayed an increase in the average tensile modulus with an increase in testing rate.

3.5. Fracture Morphology. After performing the tensile testing, SEM characterized the microstructure of the nanocomposites. A layered/laminated structure with homogeneously dispersed MMT was achieved as shown in Figure 6.

The 25 vol.% MMT nanocomposite image shows a much more ordered brick and mortar structure similar to that of nacre, which Espinosa et al. [2] described as a mechanism for improving the mechanical properties of nacre. In this case, the layers observed in the PVA-MMT nanocomposites are likely stacks of individual MMT sheets that have not been fully exfoliated but are rather intercalated with PVA. The as-cast cross-sections of the nanocomposites displayed the nanoclay distribution in the PVA matrix for the different volume fractions of nanoclay loading.

4. Discussion

To further understand the role of increasing the nanoclay volume fraction on the nanocomposite mechanical response, the tensile modulus was compared to the effective tensile

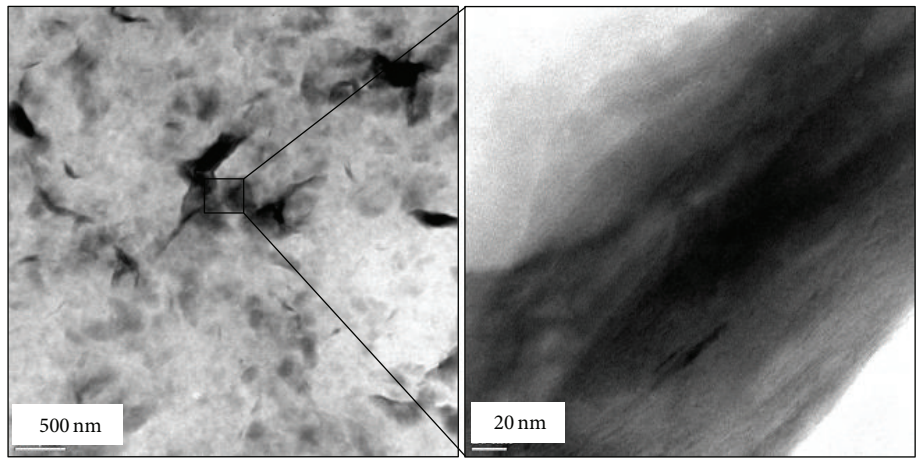

(a) (b)

Figure 3: TEM images of the 1 vol.% MMT dispersion in the PVA at (a) low magnification and (b) high magnification.

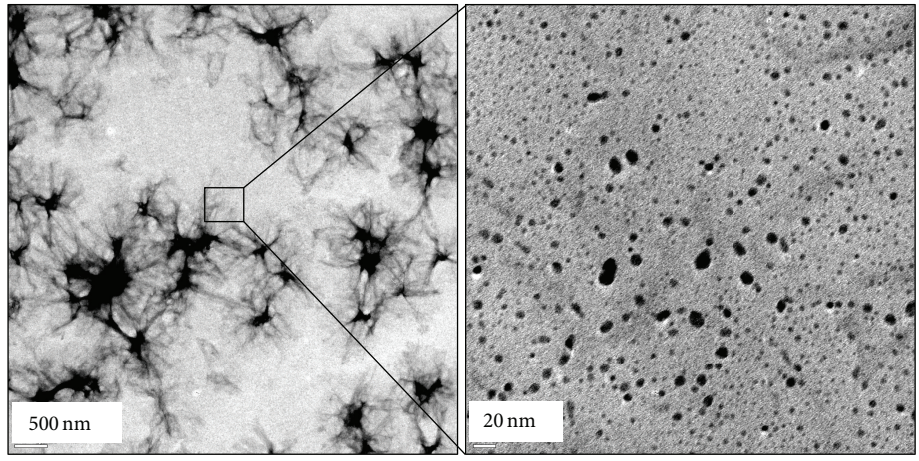

(a) (b)

Figure 4: TEM images of the 25 vol.% MMT dispersion in the PVA at (a) low magnification and (b) high magnification.

modulus estimated based on the rule of mixtures and Halpin-Tsai empirical model in Figure 7.

The equation of rule of mixtures for elastic modulus is

$$E = E_{\mathrm{MMT}}\phi_{\mathrm{PVA}} + E_{\mathrm{PVA}}\left(1 - \phi_{\mathrm{MMT}}\right), \tag{1}$$

where E is the effective tensile modulus of the composites, E_{MMT} is the elastic modulus of single MMT layer (≈160 GPa based on the value reported in [23]), E_{PVA} is the tensile modulus of PVA from experiments, and ϕ_{MMT} is the volume fraction of MMT.

The equations for Halpin-Tsai model [33] are

$$E = E_{\mathrm{PVA}}\left(\frac{1 + 2\left(L/t\right)\phi_{\mathrm{MMT}}\eta}{1 - \phi_{\mathrm{MMT}}\eta}\right),$$
$$\eta = \frac{\left(E_{\mathrm{MMT}}/E_{\mathrm{PVA}}\right) - 1}{\left(E_{\mathrm{MMT}}/E_{\mathrm{PVA}}\right) + 2\left(L/t\right)}, \tag{2}$$

where L is the length of MMT single layer (≈100 nm) and t is the thickness of MMT single layer (≈1 nm).

The graph in Figure 7 shows that, at lower volume fractions of nanoclay, the experimental results are very similar to that of the empirical models. At 25 vol.% MMT nanoclay, the nanocomposites show a higher discrepancy with the numerical values determined by the models' equations. This discrepancy is assumed to be due to a nonhomogeneous dispersion of the clay on the polymer matrix. It is believed that, at higher volume fractions of MMT, a more uniform distribution of the clay in the material is more difficult to achieve, thus reducing the effectiveness of the MMT at improving mechanical response.

Additionally, the tensile results were converted to MMT weight% in order to be compared to published data of PVA and MMT nanocomposites (Figure 8).

In Figure 8, the MMT content varied from 0 wt.% to 38.28 wt.% (25 vol.%), and there was also a difference in displacement rates used for testing and synthesis methods

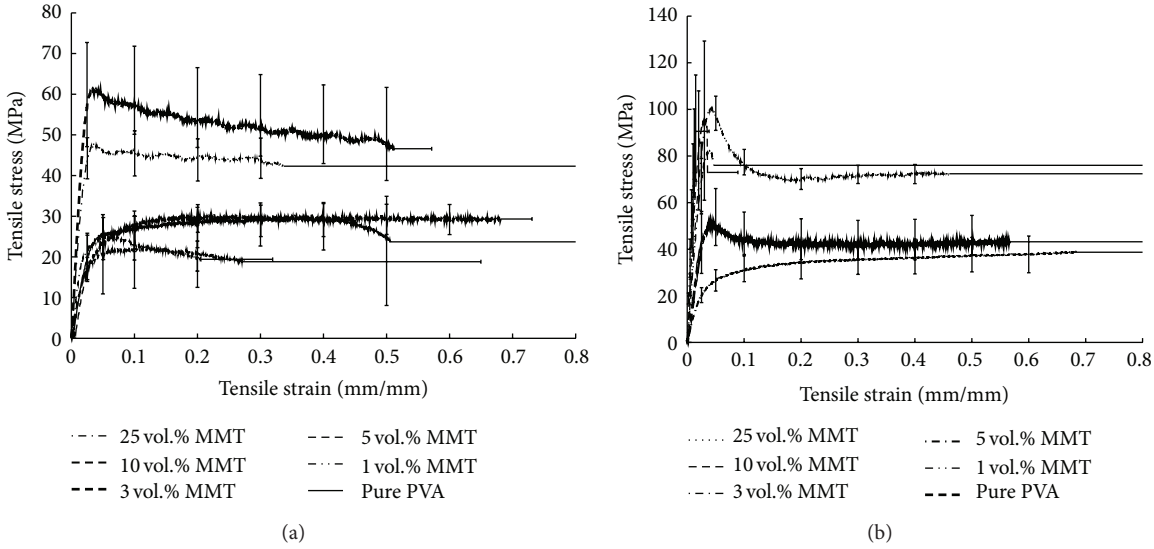

Figure 5: Tensile stress-strain behavior of the nanocomposites at displacement rates of (a) 1 mm/min and (b) 50 mm/min. Note that the error bars illustrate not only the uncertainty in the hardening and recovery but the failure strain as well. For samples that did not fracture, the failure strain uncertainty band extends off the x-axis of the plot.

Table 2: Comparison of maximum, minimum, average, and one standard deviation (STD dev.) of the mean for the tensile modulus data tested at 1 mm/min and 50 mm/min.

Value	Pure PVA	1 vol. %	3 vol. %	5 vol. %	10 vol. %	25 vol. %	Rate (mm/min)
Maximum (MPa)	1502	2750	3631	1539	1039	1913	1.0
Minimum (MPa)	792	2211	2940	526	812	1183	
Average (MPa)	1072	2431	3233	1018	928	1564	
STD dev.	378	283	358	507	114	366	
Maximum (MPa)	2572	4096	3346	1379	6501	8884	50.0
Minimum (MPa)	1671	3251	2671	1071	3640	4979	
Average (MPa)	2064	3640	2966	1195	5055	6919	
STD dev.	462	425	345	162	1403	1952	

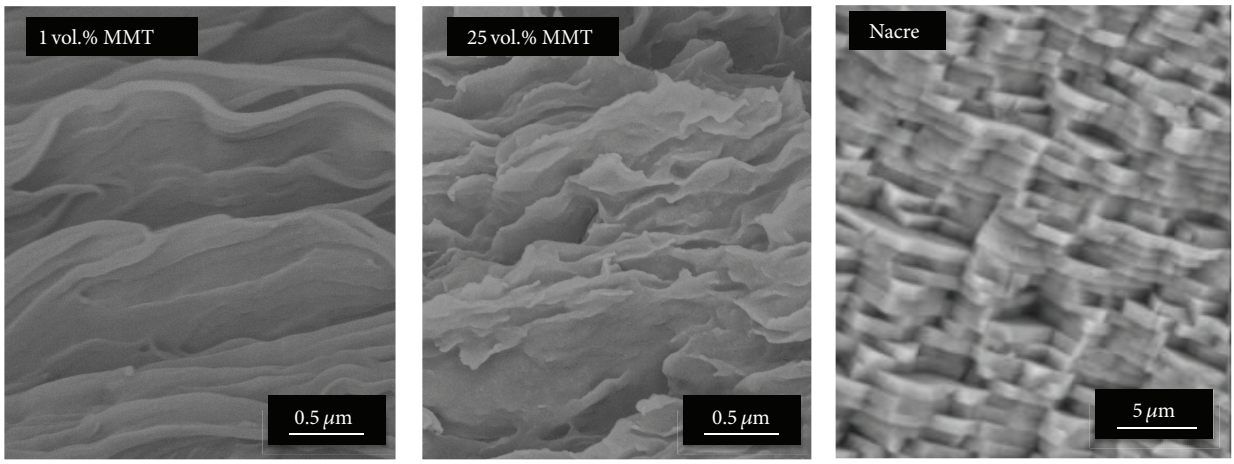

Figure 6: SEM image comparison of 1 and 25 vol.% MMT microstructure to nacre microstructure.

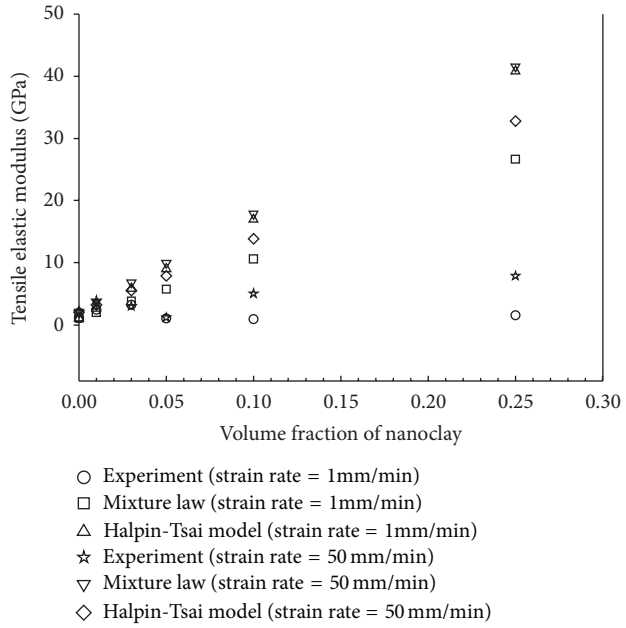

Figure 7: Comparison of experimental tensile modulus to empirical models.

of the PVA and MMT nanocomposites. Displacement rates of 18 mm/min used by Soundararajah et al. [29] and rates of 50 mm/min used by Wang et al. [30] were compared to the 1 mm/min and 50 mm/min examined in this study.

Soundararajah et al. [29] prepared the samples by solid-state shear milling that oriented and exfoliated the MMT layers along the injection molding direction. The tensile results by Soundararajah et al. [29] exhibited less scatter than the solution-intercalation film cast samples by Soundararajah et al. or the modified solution-intercalation method samples presented in this research.

Due to the difference in testing rates between Zhu et al. [28] and this study it is difficult to make a direct comparison since the tensile data from this research shows that UTS is affected by loading rate. However, trends in increasing MMT content are visible with Zhu et al. [28] showing a maximum UTS at 4 wt.% MMT. Soundararajah et al. [29] also report the highest UTS around this range for the solid-state shear milled samples at 3 wt.% MMT. The results from these researchers correlate to the UTS data presented in this study, which exhibited two UTS peaks, with the first UTS peak around 1.84 wt.% MMT and another UTS peak at higher 38.28 wt.% MMT that was not tested by the other researchers. This suggests that even for varying synthesis methods higher UTS for the nanocomposites may be obtained through possible mechanisms of optimal dispersion and exfoliation between the 1.84 and 4 wt.% MMT concentrations that do not appear to be loading rate dependent. XRD and TEM results correlate to this optimal dispersion and exfoliation where at the lower clay volume fractions the PVA is able to intercalate into the interlayer of the clay, which contributed to an increased d-spacing of 1.8 nm for the 1 and 3 vol.% MTT samples for this study. Additionally, the comparison of the TEM images for the 1 and 25 vol.% MMT in Figure 4 clearly identifies that dispersion was much better at the lower clay content, while the higher clay content depicted large quantities of agglomeration. At the higher strain rate, these strengthening mechanisms are shown to be less important since the ultimate tensile strengths are very similar to the 1, 3, 10, and 25 vol.% MMT samples. However, these microstructural features at higher clay volume fractions show strong rate dependence on elongation with the 10 and 25 vol.% samples exhibiting tensile strains less than 0.1 mm/mm for the higher rate, while the lower rate allowed for much larger strain to failures between 0.25 and 0.7 mm/mm. Therefore, indicating the damage evolution is much more influenced by loading rate for the higher clay volume fractions.

5. Conclusions

The experimental parameters that varied in this analysis included different volume fractions of nanoclay and different tensile displacement rates. Analyses consisted of uniaxial tensile testing, measurements of thermal properties, characterization of microstructure, and failure morphology and comparisons between experimental and empirical results. Clear differences in the mechanical and thermal responses were observed from the pure PVA to the 25 vol.% MMT samples. Specifically, some of the experimental observations include the following.

(1) TGA decomposition rate decreased as MMT concentration increased, which is attributed to the thermal stability of the MMT reinforcing particles and their influence on the thermal stability of the PVA.

(2) Typical higher flow/yield stresses were observed as the testing rate increased.

(3) At the lower loading rate (1 mm/min) used in this study, only the nanocomposites made at lower loading levels of clay (1 vol.% and 3 vol.% MMT) show a significant improvement on tensile strength over pure PVA. At higher loading rate (50 mm/min), the nanocomposites with all volume fractions of MMT investigated, except 5 vol.% MMT, show improvements on tensile strength over pure PVA.

(4) Microstructure of the higher volume fraction MMT samples was highly laminated and was more representative of the nacreous brick and mortar microstructure.

(5) TEM investigations of the dispersion of the MMT in the matrix identified more agglomerated particles at higher volume fraction, which may act as larger particles causing the lower strengths for the higher volume fractions.

Overall, these results suggest that the mechanical properties of PVA/MMT nanocomposites can be increased until the point that agglomeration of the clay limits its ability to be fully exfoliated in the polymeric matrix. Further research to improve synthesis processes, in particular for high volume fractions of MMT, is necessary.

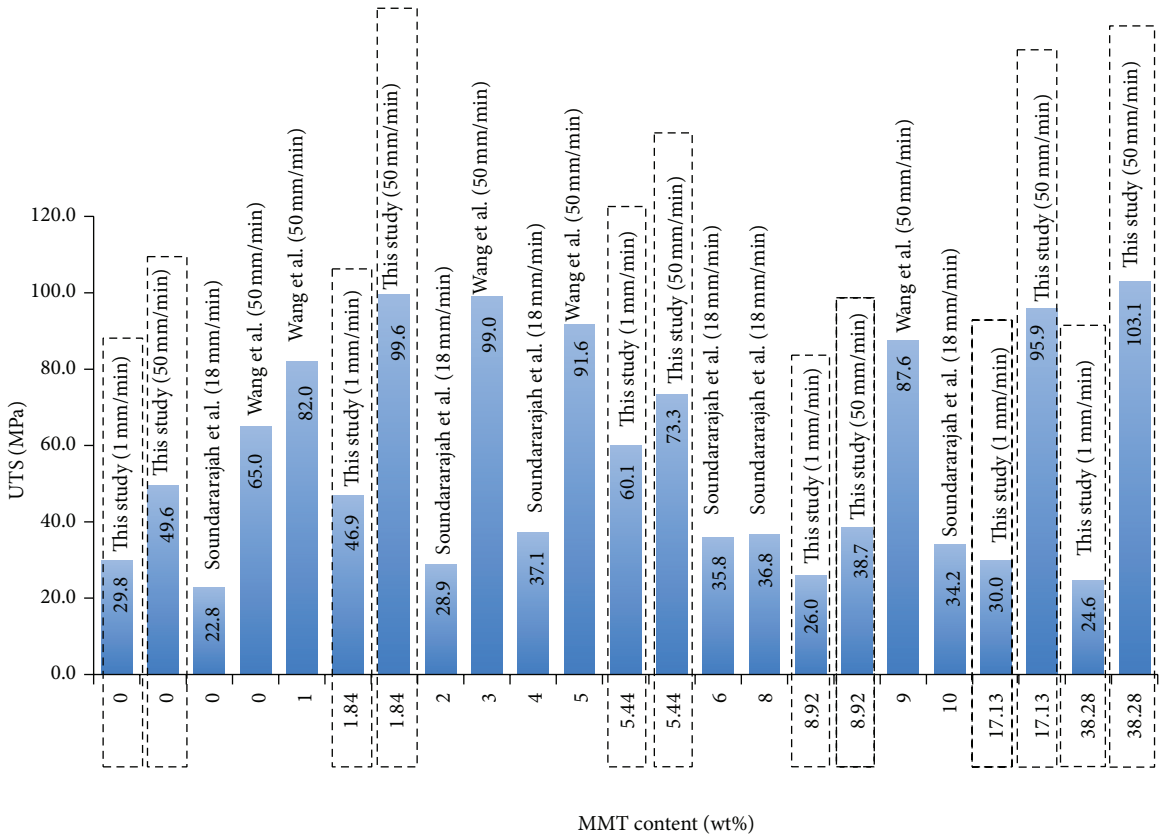

Figure 8: Average ultimate tensile strength data compared to published values [29, 30] as a function of MMT content (wt.%).

Conflict of Interests

The authors declare that there is no conflict of interests regarding the publication of this paper.

Acknowledgments

The authors would like to acknowledge funding provided for this work by the Center-Directed Research Program, US Army Engineer Research and Development Center. Permission to publish was granted by Director of Geotechnical and Structures Laboratory.

References

[1] X. Li, Z.-H. Xu, and R. Wang, "In situ observation of nanograin rotation and deformation in nacre," *Nano Letters*, vol. 6, no. 10, pp. 2301–2304, 2006.

[2] H. D. Espinosa, J. E. Rim, F. Barthelat, and M. J. Buehler, "Merger of structure and material in nacre and bone—perspectives on de novo biomimetic materials," *Progress in Materials Science*, vol. 54, no. 8, pp. 1059–1100, 2009.

[3] F. Barthelat, H. Tang, P. D. Zavattieri, C.-M. Li, and H. D. Espinosa, "On the mechanics of mother-of-pearl: a key feature in the material hierarchical structure," *Journal of the Mechanics and Physics of Solids*, vol. 55, no. 2, pp. 306–337, 2007.

[4] P. G. Allison, J. F. Deang, A. J. Diaz et al., "Characterization of paddlefish (*Polyodon spathula*) rostrum stellate bones," *Bioinspired, Biomimetic and Nanobiomaterials*, vol. 3, no. 1, pp. 63–68, 2013.

[5] J. McKittrick, P.-Y. Chen, L. Tombolato et al., "Energy absorbent natural materials and bioinspired design strategies: a review," *Materials Science and Engineering C*, vol. 30, no. 3, pp. 331–342, 2010.

[6] M. W. Trim, M. F. Horstemeyer, H. Rhee et al., "The effects of water and microstructure on the mechanical properties of bighorn sheep (*Ovis canadensis*) horn keratin," *Acta Biomaterialia*, vol. 7, no. 3, pp. 1228–1240, 2011.

[7] P. G. Allison, M. Q. Chandler, R. I. Rodriguez et al., "Mechanical properties and structure of the biological multilayered material system, *Atractosteus spatula* scales," *Acta Biomaterialia*, vol. 9, no. 2, pp. 5289–5296, 2013.

[8] P. G. Allison, R. I. Rodriguez, R. D. Moser et al., "Characterization of multi-layered fish scales (*Atractosteus spatula*) using nanoindentation, X-ray CT, FTIR, and SEM," *Journal of Visualized Experiments*, no. 89, Article ID e51535, 2014.

[9] M. Q. Chandler, P. G. Allison, R. I. Rodriguez, R. D. Moser, and A. J. Kennedy, "Finite element modeling of multilayered structures of fish scales," *Journal of the Mechanical Behavior of Biomedical Materials*, vol. 40, pp. 375–389, 2014.

[10] A. Marino Cugno Garrano, G. La Rosa, D. Zhang et al., "On the mechanical behavior of scales from *Cyprinus carpio*," *Journal of*

the Mechanical Behavior of Biomedical Materials, vol. 7, pp. 17–29, 2012.

[11] H. Gao, "Application of fracture mechanics concepts to hierarchical biomechanics of bone and bone-like materials," *International Journal of Fracture*, vol. 138, no. 1–4, pp. 101–137, 2006.

[12] Y. Turhan, Z. G. Alp, M. Alkan, and M. Doğan, "Preparation and characterization of poly(vinylalcohol)/modified bentonite nanocomposites," *Microporous and Mesoporous Materials*, vol. 174, pp. 144–153, 2013.

[13] T. M. Pique, C. J. Perez, V. A. Alvarez, and A. Vazquez, "Water soluble nanocomposite films based on poly(vinyl alcohol) and chemically modified montmorillonites," *Journal of Composite Materials*, vol. 48, no. 5, pp. 545–553, 2014.

[14] E. Dunkerley, H. Koerner, R. A. Vaia, and D. Schmidt, "Structure and dynamic mechanical properties of highly oriented PS/clay nanolaminates over the entire composition range," *Polymer*, vol. 52, no. 4, pp. 1163–1171, 2011.

[15] C. M. Paranhos, K. Dahmouche, S. Zaioncz, B. G. Soares, and L. A. Pessan, "Relationships between nanostructure and thermomechanical properties in poly(vinyl alcohol)/montmorillonite nanocomposite with an entrapped polyelectrolyte," *Journal of Polymer Science Part B: Polymer Physics*, vol. 46, no. 23, pp. 2618–2629, 2008.

[16] P. Podsiadlo, A. K. Kaushik, E. M. Arruda et al., "Ultrastrong and stiff layered polymer nanocomposites," *Science*, vol. 318, no. 5847, pp. 80–83, 2007.

[17] A. Sarfraz, M. F. Warsi, M. I. Sarwar, and M. Ishaq, "Improvement in tensile properties of PVC-montmorillonite nanocomposites through controlled uniaxial stretching," *Bulletin of Materials Science*, vol. 35, no. 4, pp. 539–544, 2012.

[18] V. Selvakumar, K. Palanikumar, and K. Palanivelu, "Studies on mechanical characterization of polypropylene/Na^+-MMT nanocomposites," *Journal of Minerals and Materials Characterization and Engineering*, vol. 9, no. 8, pp. 671–681, 2010.

[19] K. E. Strawhecker and E. Manias, "Structure and properties of poly(vinyl alcohol)/Na^+ montmorillonite nanocomposites," *Chemistry of Materials*, vol. 12, no. 10, pp. 2943–2949, 2000.

[20] J. Wang, Q. Cheng, L. Lin, L. Chen, and L. Jiang, "Understanding the relationship of performance with nanofiller content in the biomimetic layered nanocomposites," *Nanoscale*, vol. 5, no. 14, pp. 6356–6362, 2013.

[21] Y. Xu, W. Hong, H. Bai, C. Li, and G. Shi, "Strong and ductile poly(vinyl alcohol)/graphene oxide composite films with a layered structure," *Carbon*, vol. 47, no. 15, pp. 3538–3543, 2009.

[22] P. Allison, R. Moser, J. Schirer, R. Martens, J. Jordon, and M. Chandler, "In-situ nanomechanical studies of deformation and damage mechanisms in nanocomposites monitored using scanning electron microscopy," *Materials Letters*, vol. 131, pp. 313–316, 2014.

[23] O. L. Manevitch and G. C. Rutledge, "Elastic properties of a single lamella of montmorillonite by molecular dynamics simulation," *The Journal of Physical Chemistry B*, vol. 108, no. 4, pp. 1428–1435, 2004.

[24] G. D. Zartman, H. Liu, B. Akdim, R. Pachter, and H. Heinz, "Nanoscale tensile, shear, and failure properties of layered silicates as a function of cation density and stress," *The Journal of Physical Chemistry C*, vol. 114, no. 4, pp. 1763–1772, 2010.

[25] A. A. Sapalidis, F. K. Katsaros, T. A. Steriotis, and N. K. Kanellopoulos, "Properties of poly(vinyl alcohol)-Bentonite clay nanocomposite films in relation to polymer-clay interactions," *Journal of Applied Polymer Science*, vol. 123, no. 3, pp. 1812–1821, 2012.

[26] A. Walther, I. Bjurhager, J.-M. Malho et al., "Large-area, lightweight and thick biomimetic composites with superior material properties via fast, economic, and green pathways," *Nano Letters*, vol. 10, no. 8, pp. 2742–2748, 2010.

[27] Y. Zhao, J. Zhai, S. Tan, L. Wang, L. Jiang, and D. Zhu, "TiO_2 micro/nano-composite structured electrodes for quasi-solid-state dye-sensitized solar cells," *Nanotechnology*, vol. 17, no. 9, pp. 2090–2097, 2006.

[28] W. Zhu, C.-H. Lu, F.-C. Chang, and S.-W. Kuo, "Supramolecular ionic strength-modulating microstructures and properties of nacre-like biomimetic nanocomposites containing high loading clay," *RSC Advances*, vol. 2, no. 15, pp. 6295–6305, 2012.

[29] Q. Y. Soundararajah, B. S. B. Karunaratne, and R. M. G. Rajapakse, "Mechanical properties of poly(vinyl alcohol) montmorillonite nanocomposites," *Journal of Composite Materials*, vol. 44, no. 3, pp. 303–311, 2010.

[30] B. Wang, Q. Wang, and L. Li, "Morphology and properties of poly(vinyl alcohol)/MMT nanocomposite prepared by solid-state shear milling (S^3M)," *Journal of Macromolecular Science B: Physics*, vol. 53, no. 1, pp. 78–92, 2014.

[31] Z. Peng and L. X. Kong, "A thermal degradation mechanism of polyvinyl alcohol/silica nanocomposites," *Polymer Degradation and Stability*, vol. 92, no. 6, pp. 1061–1071, 2007.

[32] K. H. Ip, B. H. Stuart, P. S. Thomas, and A. Ray, "Characterisation of poly(vinyl alcohol)-montmorillonite composites with higher clay contents," *Polymer Testing*, vol. 30, no. 7, pp. 732–736, 2011.

[33] J. C. Halpin and J. L. Kardos, "The Halpin-Tsai equations: a review," *Polymer Engineering and Science*, vol. 16, no. 5, pp. 344–352, 1976.